A New Acoustic Emission Sensor Based Gear Fault Detection Approach

Yongzhi Qu[1], Eric Bechhoefer[2], David He[1], and Junda Zhu[1]

[1]*Department of Mechanical and Industrial Engineering, University of Illinois at Chicago, Chicago, IL, 60607, USA*
davidhe@uic.edu

[2]*NRG Systems, Hinesburg, VT, 05461, USA*
erb@nrgsystems.com

ABSTRACT

In order to reduce wind energy costs, prognostics and health management (PHM) of wind turbine is needed to reduce operations and maintenance cost of wind turbines. The major cost on wind turbine repairs is due to gearbox failure. Therefore, developing effective gearbox fault detection tools is important in the PHM of wind turbine. PHM system allows less costly maintenance because it can inform operators of needed repairs before a fault causes collateral damage happens to the gearbox. In this paper, a new acoustic emission (AE) sensor based gear fault detection approach is presented. This approach combines a heterodyne based frequency reduction technique with time synchronous average (TSA) and spectral kurtosis (SK) to process AE sensor signals and extract features as condition indictors for gear fault detection. Heterodyne techniques commonly used in communication are used to preprocess the AE signals before sampling. By heterodyning, the AE signal frequency is down shifted from MHz to below 50 kHz. This reduced AE signal sampling rate is comparable to that of vibration signals. The presented approach is validated using seeded gear tooth crack fault tests on a notational split torque gearbox. The approach presented in this paper is physics based and the validation results have showed that it could effectively detect the gear faults.

1. INTRODUCTION

The largest variable cost to owners and operators of wind turbines is unscheduled maintenance. PHM has been shown to be technique that can successfully reduce both scheduled and unscheduled maintenance. PHM system allows better maintenance practices as well as less costly maintenance because it can give indications and warnings prior to collateral damage occurring. In wind turbines, this might be the difference between an up tower maintenance effect or a down tower event, which requires a crane (a large fixed expense). Or, it could be the difference between refurbishing a gearbox instead of replacing it. Therefore the development of effective gearbox fault detection tools is important to the PHM of wind turbine. Currently, vibration is the most widely used tool in diagnosis of machine fault, such as: shaft, gears, and bearings. Common vibration sensors include accelerometer, displacement and velocity sensors. However, vibration signals have some drawbacks when it comes to detecting the incipient machine faults at low frequency. Accelerometers measure the second derivative of the displacement. For low frequency components, such as the carrier or planets, which operate below 2 Hz, even damage components may develop acceleration below the noise floor of the sensor. AE, on the other hand, does not measure acceleration and is not a function of displacement: it is independent of shaft rate. This has been observed in (Al-Ghamd & Mba, 2006), where early fault signatures were not present in vibration data, but was detected by AE. If these faults could be detected at an early stage, significant maintenance costs could be saved. In this paper, the development of a new AE sensor based gear fault detection approach is presented.

AE is commonly defined as transient elastic waves within a material, caused by the release of localized stress energy. It is produced by the sudden internal stress redistribution of material because of the changes in the internal structure of the material. Possible causes of these changes are crack initiation and growth, crack opening and closure, or pitting in various monolithic materials (gear, bearing material) or composite materials (concrete, fiberglass). Thus the ability to detect AE can be used to give diagnostics indications of component health. The challenges of using AE sensor include: the frequency of the output signals from AE sensor is generally high, even as high as several MHz. Thus a high sampling rate between 2MHz and 10MHz is normally

needed for AE data collection. Other challenges include the high data volume, complicated feature of AE signals, which make the data processing highly difficult.

A number of methods have been developed for AE signal analysis, but few techniques have been successful in application. Most of the research into AE for machine condition monitoring focuses on time domain features, such as: peak, total energy, standard deviation, median, AE counts, root mean square (RMS) voltage and duration (Mba, 2003). These features all relate to the absolute energy levels of the measured signals. As the absolute energy could vary from one machine to another, or vary at different locations on the same machine, the effectiveness of these features may be compromised. Consequently, these features are not ideal for fault detection purpose.

Gao *et al.* (2011) proposed a wavelet transform based method to analyze AE signals, which could act as a supplement redundant method for vibration test. He and Li (2011) developed a data mining based method to classify the condition indicators derived from different AE data to detect fault. Later, Li and He (2012) introduced an EMD-based AE feature quantification method. In their work, successful detection of gear fault was achieved on AE data sampled at a rate as low as 500 kHz. Artificial neural networks (ANN) have also been adopted for AE signal classification. In (Pandya *et al*., 2013), a supervised learning process was developed after EMD decomposition for bearing fault detection using AE signals.

In (Kilundu *et al*., 2011), cyclostationarity analysis was compared with traditional envelope spectrum. It was proposed that the cyclic spectral correlation, a tool for characterizing cyclostationarity, was more efficient compared with envelope spectrum for bearing fault diagnosis. A comparison study between vibration and AE based on spectral kurtosis was reported in (Eftekharnejad *et al*. 2011). The conclusion was that by using AE features with spectral kurtosis, the fault could be detected at an earlier stage. Al-Balushi *et al.* (2002) developed an energy based feature, named energy index. By calculating the cumulative of the square root of the energy index, the tooth fault could be identified as high peak values.

There are still a number of issues in the reviewed methods. First, the AE data was collected at very high sampling frequency, typically 2~5MHz. Second, these methods tried to detect the gear faults using data driven approach rather than physics based approach. Data driven approaches normally rely on complicated computation algorithms such as EMD and wavelet analysis to compute the AE features.

This research is aimed to address the AE sensor based gear fault detection problem using physics based methods, similar to those techniques applied to vibration signal to analyze the AE data. For gear fault detection, it is common to use time synchronous average (TSA) to extract the gear signals from the raw signals. Generally, the signals collected from a gearbox contain broadband and non-synchronous noise, such as other shaft/gear pairs, or bearing tones. TSA is able to reduce the random and non-synchronized noise from other sources while enhancing the synchronous signals from the gear of interest. In order to perform TSA on the AE signals, high sampling frequency and large data volume need to be addressed. This requires a frequency demodulation/decimation technique be applied prior to data sampling and signal analysis. The heterodyne technique is proposed to demodulate the signals and down shift the signals to a low frequency range. After the heterodyne is applied, the AE signal can be sampled at frequencies comparable to that of vibration analysis. If a phase reference is available, the TSA could be generated.

The remainder of the paper is organized as follows. Section 2 illustrates in details the methodology. In Section 3, the setup of the experiments for the validation of the methodology is explained. Section 4 presents the analysis results of the experiments and illustrates how a fault is identified. Finally, Section 5 concludes the paper.

2. THE METHODOLOGY

The methodology will be illustrated in 4 parts. The first part discusses the heterodyne technique. TSA will be briefly reviewed in the second part. The third part explains how the kurtogram could be applied and idea of designing an optimal band pass filter from spectral kurtosis. Then, condition indicators for gearboxes diagnosis are discussed.

2.1. The Heterodyne Technique

Current AE signal processing steps are given in Figure 1.

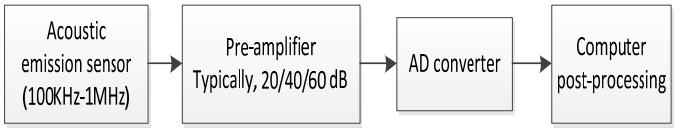

Figure 1. Traditional AE signal acquisition and preprocessing procedure

In a traditional AE signal processing procedure, all of the data is collected and stored to computer without any signal processing. There are two disadvantages associated with this procedure. First, it increases the data acquisition cost. Second, it relies on the computer to process the resulting large data set.

When taking a further look at an AE signal, one will find that the AE signal is virtually a carrier signal for the fault signal. The information of interest is related to the load signal, not the high frequency AE carrier signal. In order to get the load signal, demodulation process is required before sampling. As for rotational machine fault detection, the faults are mostly related to the rotational speed, which is generally in the low frequency range. Thus, the information

of interest is related to the low frequency load signals, not the high frequency AE carrier signal. This low frequency load information is recovered through a demodulation process. The demodulation process is similar to information retrieval in an amplitude/phase modulated radio frequency signal. The carrier signal of a typical AM radio signal is several MHz, while the information modulated onto that signal is audio signal of a couple of kHz. After demodulating the carrier using an analog signal conditioning circuit, the acquisition system can then be sampled at audio frequency (10s of kHz). This signal processing can then be performed at lower cost with an analog circuit rather than a high speed analog to digital converter and the associated computation power required to process the large data set resulting from the high sample rate.

The AE signal demodulator implemented in this paper work similarly to a radio quadrature demodulator: shifting the carrier frequency to baseband, followed by low pass filtering. The technique applied here is called heterodyne. Mathematically, heterodyning is based on the trigonometric identity. For two signals with frequency f_1 and f_2, respectively, it could be written as

$$\begin{aligned} &sin(2\pi * f_1 * t) * sin(2\pi * f_2 * t) \\ &= \frac{1}{2}cos[2\pi(f_1 - f_2)] - \frac{1}{2}cos[2\pi(f_1 + f_2)] \end{aligned} \quad (1)$$

where, f_1 is the carrier frequency, f_2 is the demodulator's reference input signal frequency. This process could be explained with a simple example.

For example, let $f_1 = 4$ Hz and $f_2 = 5$ Hz, note $y_1 = sin(2\pi * 4 * t)$ and $y_2 = sin(2\pi * 5 * t)$. Take their multiplication as $Y = y_1 .* y_2$, as shown in Figure 2.

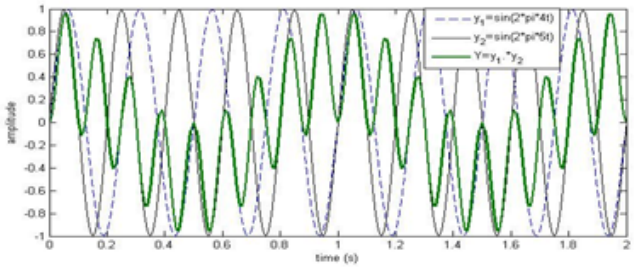

Figure 2. The multiplication of two sinusoid signals

The modulated signal is then low pass filtered to reject the high frequency image at frequency $(f_1 + f_2)$, as shown in Figure 3.

A detailed discussion of the heterodyne technique applied on the raw AE signal is given in the following. In general, amplitude modulation is the major modulation form for AE signal. Although, frequency modulation and phase modulation could present in the AE signal potentially, they are considered trivial and will not be discussed here. The amplitude modulation function is given in Eq. (2).

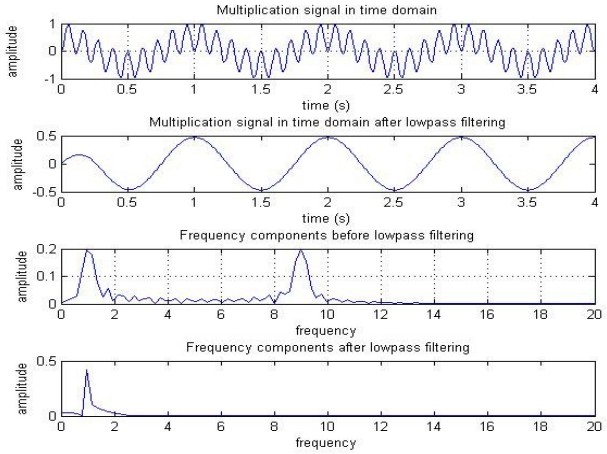

Figure 3. The extraction of the heterodyned signal by frequency domain filtering

$$U_a = (U_m + mx)co\,s\,\omega_c t \quad (2)$$

where, U_m is the carrier signal amplitude, ω_c is the carrier signal frequency, m is the modulation coefficient. x is the modulated signal, note as

$$x = X_m cos\Omega t \quad (3)$$

Then, with heterodyne technique, the modulated signal will be multiplied with a unit amplitude reference signal $\cos(\omega_c t)$. The result is given in the following.

For the amplitude modulation signal,

$$\begin{aligned} U_o &= (U_m + mx)\,cos\,\omega_c t\,cos\,\omega_c t \\ &= (U_m + mx)\left[\frac{1}{2} + \frac{1}{2}cos(2\omega_c t)\right] \end{aligned} \quad (4)$$

Then substitute Eq. (3) in into Eq. (4), it gives:

$$\begin{aligned} U_o &= \frac{1}{2}U_m + \frac{1}{2}X_m cos\Omega t + \frac{1}{2}U_m cos(2\omega_c t) \\ &+ \frac{1}{4}mX_m[cos(2\omega_c + \Omega)t + cos(2\omega_c - \Omega) \end{aligned} \quad (5)$$

Since U_m does not contain any useful information related with the modulated signal, it could be set as 0, or removed by de-trending. From Eq. (5), it can be seen that only the modulated signal will be left after low pass filtering, where the high frequency components around frequency $2\omega_c$ will be removed.

The diagram of the proposed down sampling system using heterodyne is shown in Figure 4.

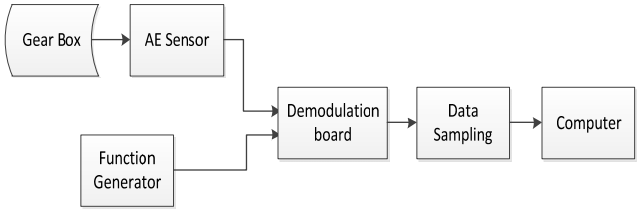

Figure 4. Proposed AE signal acquisition and preprocessing procedure

By adding a demodulation step, it could achieve the purpose of reducing the signal frequency to 10s of kHz. This is close to the frequency range of general vibration signals. Any data acquisition board with a low sampling rate could be able to sample the pre-processed AE data.

2.2. AE Signal TSA

TSA has been widely used in processing the vibration signals for rotating machine fault diagnosis (McFadden & Toozhy, 2000; Bonnardot *et al.*, 2005). The idea of TSA is to use the ensemble average of a raw signal over certain number of revolutions in order to enhanced signal of interest with less noise from other sources. For a function *x(t)*, digitized at a sampling interval *nT*, resulting in sampling in samples *x(nT)*. Denoting the averaged period by mT, TSA is given as (Braun, 1975):

$$y(nT) = \frac{1}{N}\sum_{r=0}^{N-1} x(nT - rmT) \tag{6}$$

More details about TSA could be found in (McFadden, 1987).

The successful application of TSA on vibration signal analysis provides the possibility of using it to process AE signals. Basically, two types of TSA algorithms are available in literature, i.e., TSA with tachometer, and tachometer less TSA. In comparison with TSA with tachometer, tachometer less TSA needs to estimate the angular information from the vibration data. For slow speed variation cases, time domain feature like gear meshing information could be used. However, tachometer less TSA will introduce more phase reference errors and thus have less accuracy than TSA with tachometer. In this work, TSA with tachometer is applied.

Despite of the popular application of TSA to vibration signal analysis, application of TSA to AE signal processing for gear fault diagnosis has not been reported in the literature. The complicated feature and large data volume of AE signals make it unrealistic to perform TSA algorithm directly on AE data with an on-line condition monitoring system. In this paper, the authors explore the application of TSA to AE signal analysis.

TSA enables the direct comparison of the acoustic signals produced by each tooth on the same gear over one revolution. TSA for gear diagnosis generally computes the acoustic signals of a single shaft revolution. After TSA is calculated, basically all kind of fault detection condition indicators can be evaluated on the TSA signal.

2.3. Spectral kurtosis (SK) and optimal band pass filter

The spectral kurtosis was proposed by Dwyer (1983), as a statistical tool that can be used to identify the non-Gaussian components in a signal as well as their location in the frequency domain. A more formal definition of SK was provided in (Capdevielle, 1996) from the perspective of higher-order statistics. By Capdevielle's definition, SK is the normalised fourth-order cumulant of the Fourier transform and can be used as a measure of distance of a process from Gaussianity. Therefore, it can act as a measure of the peakiness of the probability density function of the process at a frequency of f. However, SK did not draw much attention from the researchers until it was revisited and further developed by Antoni (2006). The SK of a signal $x(t)$ is defined as the energy-normalized fourth-order spectral cumulant as:

$$K_x(f) = \frac{S_{4x}(x)}{S_{2x}^2(f)} - 2 \tag{7}$$

where $S_{nx}(f) = \langle |X(t,f)|^n \rangle$, $\langle \cdot \rangle$ stands for the time averaging operator, $X(t,f)$ is the complex envelop of signal $x(t)$.

$X(t,f)$ can be estimated by any time-frequency analysis methods, such as: short time Fourier transform (STFT), the filter bank method, Wigner-Ville distribution, and wavelet package..

Take STFT for example, the STFT of signal $x(t)$ discretely sampled as $X(n)$ is defined as:

$$X_w(kP,f) = \sum_{n=-\infty}^{\infty} X(n)w(n-kP)e^{-j2\pi nf} \tag{8}$$

where, $w(n)$ is a positive analysis window, P is a given temporal step.

As noted, the SK is suitable for identifying the peakiness of a signal with regard to frequency. It is able to extract non-stationary event in the signal. In general, the vibration signals measured from rotating machinery is considered as stationary. However, an AE signal is considered non-stationary. Gear signals can be classified as cyclostationary process. As indicated in (Antoni, 2006), the signals from rotating machinery can be resynchronized with a phase reference and then form a non-stationary signal with a periodic statistical structure. It is therefore conditionally non-stationary, which is suitable to use SK for fault detection.

In order to estimate SK, the kurtogram was proposed by Antoni and Randall (2006). A kurtogram is a three

dimension graph which gives the kurtosis value for different frequency and different window size. Window size N_w is an important parameter because it directly affects the spectral resolution of the SK. A short N_w will yield high SK value, but too short a N_w will also lose some details and reduce the frequency resolution. Therefore, both the frequency and N_w should be optimized while the maximum SK can be identified. Since a kurtogram can identify the optimal frequency range and optimal window size where the signal displays the maximum peakiness, it is very useful for filter design. After the frequency line where the maximum SK is obtained, several filter methods could be applied to extract an enhanced SNR signal, such as Wiener filter, matched filter and band pass filter (Antoni & Randall 2006).

For optimal band pass filter, the objective is to find: (1) the central frequency $\boldsymbol{f_c}$ and (2) the bandwidth $\boldsymbol{B_f}$ of the filter which maximizes peakiness on the filtered signal. For fault detection problem, in order to recover the impulse associated with a faulty signature, a band pass filter which is used to maximize the kurtosis of the envelope of the filtered signal. As demonstrated in (Antoni & Randall 2006), this problem is strictly equivalent to finding the frequency $\boldsymbol{f}$ and the window length $\boldsymbol{N_w}$ that maximises the STFT-based SK over all possible combinations. The optimal central frequency $\boldsymbol{f_c}$ and bandwidth $\boldsymbol{B_f}$ of the band pass filter are determined as those values which jointly maximize the kurtogram. Therefore, both the center frequency $\boldsymbol{f_c}$ and window length $\boldsymbol{N_w}$ could be identified by using kurtogram. By doing this, the best compromise between maintaining the highest possible signal to noise ratio and extracting the impulse like signature of the fault is achieved.

2.4. Condition indicators for gearboxes diagnosis

Many vibration based condition indicators for gear fault detection have been reported in literature. Most of the condition indicators deal with the data distribution, such as peakiness, amplitude level, deviation from the mean and so on. A major difference between these condition indicators lies in the signal from which they are calculated. Generally four types of signals are used for computation, i.e., raw signals, time synchronous average signals, residual signasl and difference signals (Večeř *et al.* 2005; Lebold *et al.* 2000). A residual signal is generally defined as a synchronous averaged signal with the shaft, gear mesh, and their associated harmonic frequencies removed (Zakrajsek, 1993). The difference signal is defined by further removing the first order sidebands from the residual signal (e.g. the distinction between the residual and difference signals is the first order sidebands). For this filtering process, the spectrum values corresponding to these features are set to zero and the inverse Fourier transform is performed to convert it back to the time domain. However, these definitions are not strict. Also in practice, different filtering methods of performing the above mentioned process will give different results.

Other operations on the TSA include:

Teager's Energy Operator: Teager's energy operator is a type of residual of the autocorrelation function (Kaiser, 1990; Teager, 1992). For a nominal gear, the predominant vibration is gear mesh. Surface disturbances, scuffing, and etc., generate small higher frequency values which are not removed by autocorrelation. The CIs of the EO are the standard statistics of the EO vector. The mathematics formula is as follows:

$$\psi[x_i] = x_i^2 - x_{i-1} \cdot x_{i+1} \tag{9}$$

where $\psi[x_i]$ is the ith element in EO, x_i is the i^{th} element of x.

Statistics are performed on the analysis, which include:

RMS: The root mean square (RMS) for a discretize sampled signal is defined as:

$$x_{rms} = \sqrt{\frac{1}{N}\sum_{i=1}^{N}(x_i{}^2)} \tag{10}$$

where x_{rms} is the root mean square value of data set x, x_i is the i-th element of x, N is the length of data set x.

From the definition of RMS, it is easy to understand that the RMS may not increase greatly with isolated peaks in the signal, and consequently it is not sensitive to incipient tooth crack or initial failure. Its value will increase as the speed and load increase.

Crest factor: Before crest factor could be defined, peak value must be understood. Peak value generally refers to the maximum value in the collected data. The crest factor then could be given in Eq. (11)

$$CF = \frac{|x|_{peak}}{x_{rms}} \tag{11}$$

where CF is the crest factor, $|x|_{peak}$ is the peak amplitude in data x, x_{rms} is the RMS.

This parameter is more sensitive to initial gear fault, such as one tooth crack. Since the RMS will not change in incipient fault, but the crest factor should see an increase.

Kurtosis: kurtosis describe how peaky or how smooth of the amplitude of data set x. If a signal contains sharp peaks with high values generated by a fault in the gearbox, it is expected that its distribution function will be sharper. Thus, the kurtosis of the fault signal should be higher than that of the healthy signal. The function of kurtosis is given below,

$$Kurt = \frac{N\sum_{i=1}^{N}(x_i - \bar{x})^4}{(\sum_{i=1}^{N}(x_i - \bar{x})^2)^2} \quad (12)$$

where *Kurt* is the kurtosis of data set x, x_i is the *i*-th element of x, *N* is the length of data set x.

It is worth to mention that for any normal distribution, the kurtosis value is 3. This could be easily verified by the moment generating function.

Some other gear fault algorithms are functions of operations, such as:

FM4: The FM4 parameter is simply the kurtosis of the difference signal. It is assumed that a healthy gearbox difference signal should display a Gaussian amplitude distribution, while a damaged gearbox will produce some high peak value which does not conform to Gaussian distribution.

$$FM4 = \frac{N\sum_{i=1}^{N}(d_i - \bar{d})^4}{(\sum_{i=1}^{N}(d_i - \bar{d})^2)^2} \quad (13)$$

where d_i is the *i*-th element of the difference signal, *N* is the length of difference signal.

NA4: NA4 is an improved version of FM4. NA4 is based on the argument that sideband signal contains the fault related information. So, the NA is calculated based on the residual signal which keeps the sideband while removing other meshing components. Also, NA4 takes an average value of the variance. The NA4 formula is given as:

$$NA4 = \frac{N\sum_{i=1}^{N}(r_i - \bar{r})^4}{(\frac{1}{M}\sum_{j=1}^{M}\sum_{i=1}^{N}(r_{ij} - \bar{r}_j)^2)^2} \quad (14)$$

where r_i is the *i*-th data point in the residual signal, r_{ij} is the *i*-th data point of the *j*-th group of residual signal, *M* is number of the data group of TSA residual signal, *N* is the number of data point in one TSA residual signal.

Figure 5 shows the overall process of computing the condition indictors using the presented approach.

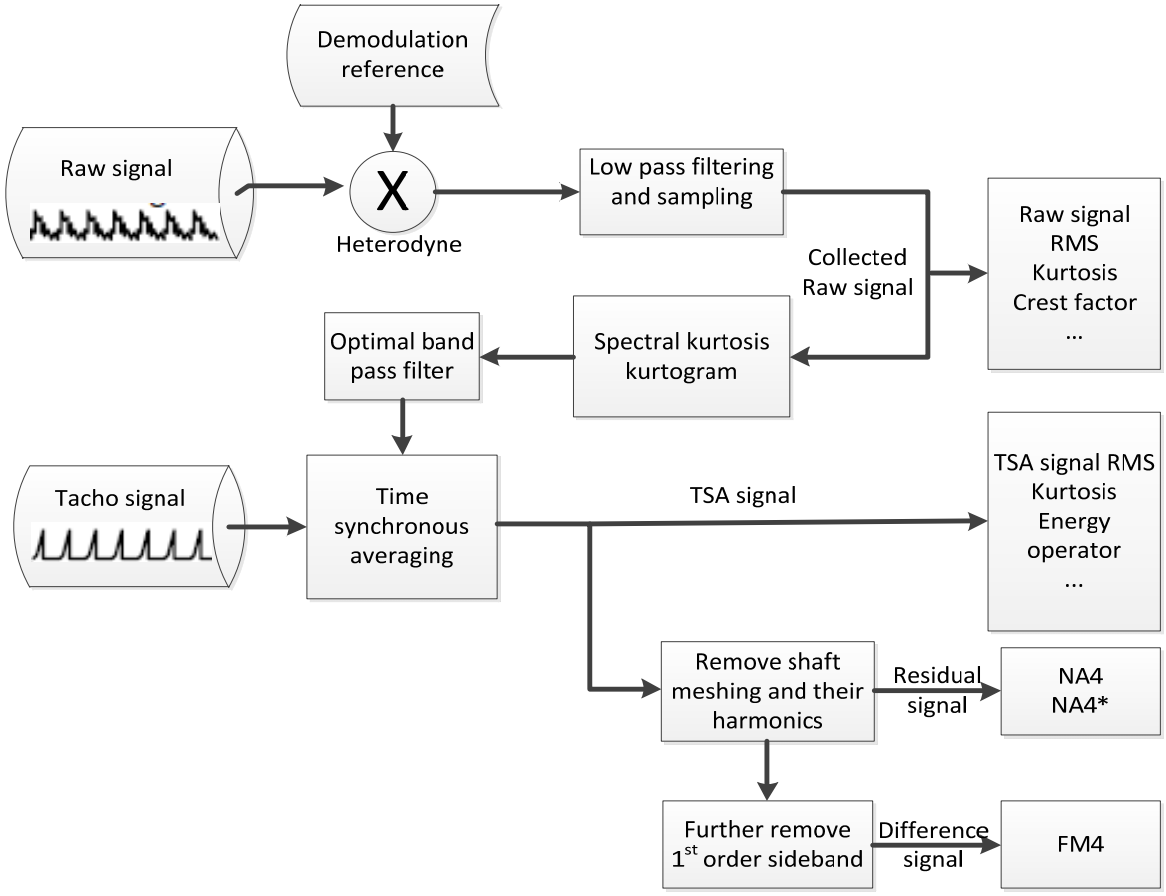

Figure 5. The overall process of computing the condition indicators

3. EXPERIMENTAL SETUP

In this section, the experiment setup for validating the AE sensor based gear fault detection approach is explained. In Figure 6, the demodulation board (Analog devices - AD8339) and sampling devices (NI-DAQ 6211) are shown. The demodulation board performed the multiplication of sensor signals and reference signals. It is an analog device and much more affordable than a high sampling rate board. It takes two inputs, one from the AE sensor, and the other from function generator as reference signal. The basic principle of AD8339 could be explained by Gilbert cell mixers. In electronics, the Gilbert cell is commonly used as an analog multiplier and frequency mixer. The output current of this circuit is an accurate multiplication of the base currents of the both inputs. According to Eq. (1) it could convert the signal to baseband and twice the carrier frequency. The output of the demodulation board goes to the sampling board and the high frequency component is filtered out. NI-DAQ 6211 is a low frequency data acquisition device, with a sample frequency up to 250kS/s. Before data acquisition, another task was to determine the frequency of the reference signal for demodulation. The objective was to down shift the AE signal frequency as low as possible. In order to remove the carrier frequency, the reference signal frequency needs to be as close to the AE carrier frequency as possible. Thus, the next step was to identify the AE sensor response frequency.

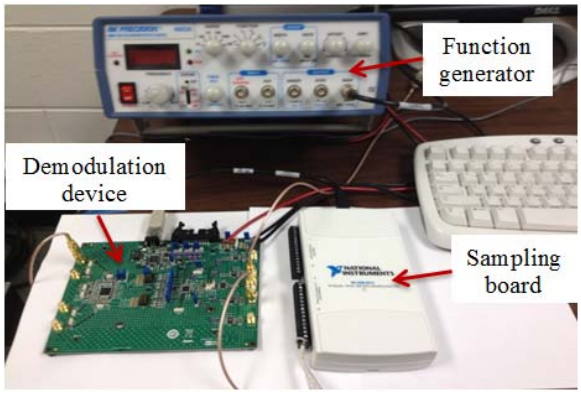

Figure 6. Demodulation device and data sampling board

Each AE sensor has its specific frequency response range, which further depends on the system being sensed and the sensor itself. With reference to the AE sensor user manual, a coarse range of the sensor response frequency is given. In order to identify a more accurate AE sensor response frequency, a function generator with sweep function was used to test the system and record the output. With a wide range of sweep frequency signal as the reference signal to demodulation board, the demodulation result varies accordingly. As mentioned before, the energy impact information of AE sensor is carried by a high frequency modulated signal. If the AE signal is successfully demodulated, most of the energy related signal will be shifted to below 50kHz, and thus it will be captured by the low frequency sampling board, which is set at 100kHz sampling rate. Otherwise most energy related information will still dwell in high frequency and therefore would be lost after low pass filtering. Using swept frequency input, one can analyze the energy envelope of the signal at different frequencies. Then the AE sensor response frequency is identified in the demodulated AE signal having the largest energy level. By this method, the accurate frequency range of the sensor output could be found. In the conducted experiment, 400 kHz was identified as the AE carrier signal center frequency. This frequency was then used as the demodulation reference frequency.

Seeded gear tooth crack fault tests were conducted on a notational two-stage split torque gearbox. The gearbox and the AE sensor location on the gearbox are shown in Figure 7.

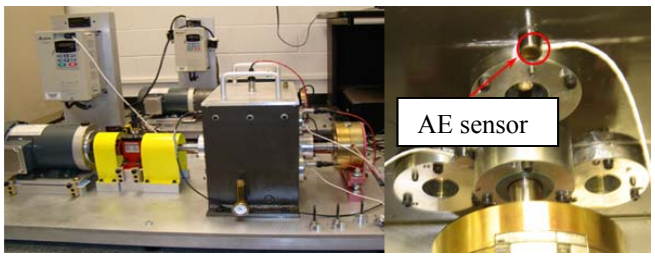

Figure 7. The notational split torque gearbox and the AE sensor location

As shown in Figure 8, the notational split torque gearbox has an intermediate stage which could split the torque and change the transmission ratio between input and output shaft.

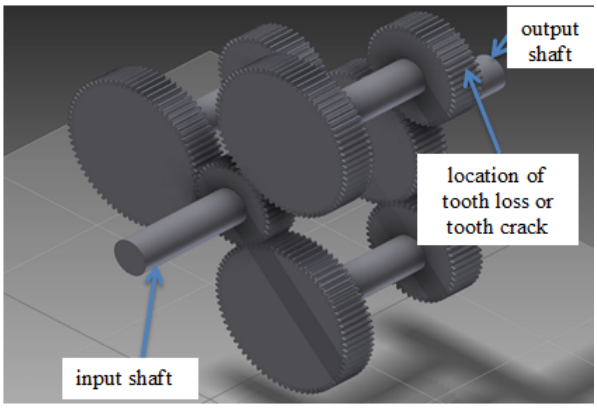

Figure 8. The structure of the notational split torque gearbox

For the faulty gearbox, one of the intermediate gears with 48 teeth was damaged by cutting the root of a gear tooth with a depth equal to half width of the gear tooth by EDM (electric discharge machining) with a wire of 0.5 mm diameter, to simulate the root crack damage in real applications. The seeded tooth crack is shown in Figure 9.

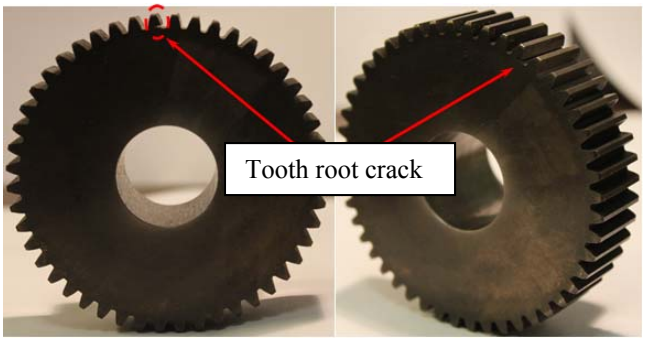

Figure 9. Seeded tooth root crack

Since this is a speed reduction gearbox, the input side and the output side have a 2.4 times speed reduction ratio. The corresponding output shaft speed and intermediate shaft (faulty gear shaft) speed are provided in Table 1.

Table 1. Output shaft speed corresponding to input shaft speed

Input shaft speed (Hz)	10	20	30	40	50	60
Faulty gear shaft frequency	5.56	11.1	16.7	22.2	27.8	33.3
Output shaft speed	4.17	8.33	12.5	16.7	20.8	25

For signal acquisition, Labview signal express software was used. During the experiments, continuous AE signals were collected. The data sampling rate was set to 100 kHz for all the tests. There was no torque load during the test. The gearbox input shaft speed is running from 10Hz-60Hz with 10Hz interval. For each speed, 5 data sets are collected. It should be noted that with a load, the faulty gear feature will be larger due to the increased impact on the gear. It is hypothesized that with a higher load, the faulty feature in AE could be more easily detected. In zero loading experiments, the identification of gear fault is more challenging than loaded cases.

4. RESULTS

The AE data after heterodyning were collected by a low sampling rate device, with the sampling rate fixed at 100 kHz. Additionally, the tachometer signals were collected together with the AE data from the main input shaft, which were used to perform the TSA calculation. Two collected examples of faulty AE data and healthy AE data are shown in Figure 10. For simplicity, the tachometer signals are not shown in the figure.

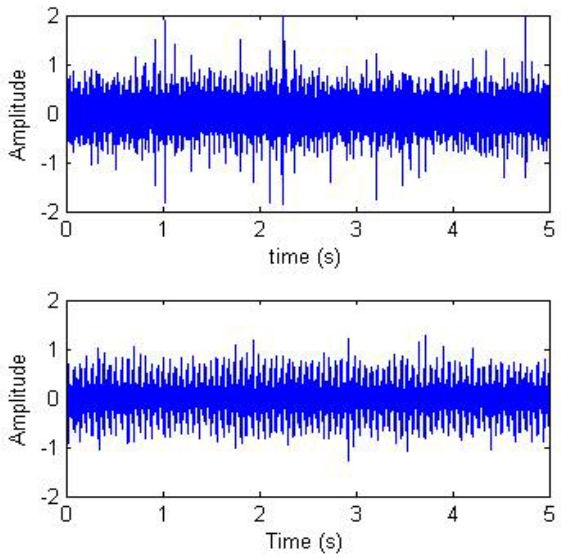

Figure 10. Healthy (upper) and faulty AE signals (lower) collected with heterodyne

Before performing TSA, the data was first analyzed using kurtogram. Figure 11 shows an example of kurtogram for a faulty signal at 30Hz. Based on the kurtogram, the center frequency and bandwidth where the spectral kurtosis is maximized could be identified. An optimal band pass filter was designed to filter the signal with regard to the corresponding frequency range.

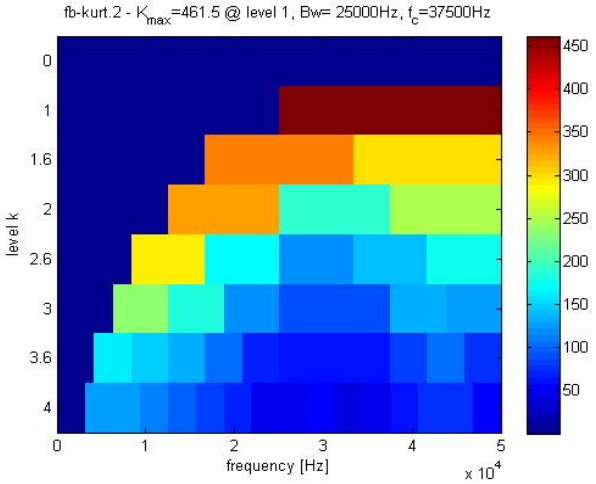

Figure 11. The kurtogram of spectral kurtosis for a faulty signal at 30Hz input shaft speed (The center frequency identified from this kurtogram is 37500Hz, with a band width of 25000Hz)

After the band pass filter, the TSA was computed using the filtered data. Since the raw signal was filtered before TSA, to maintain the phase unchanged, a zero-phase filter was used. About 260 averages were taken for each group of data. The TSA signal at 30Hz is shown in Figure 12.

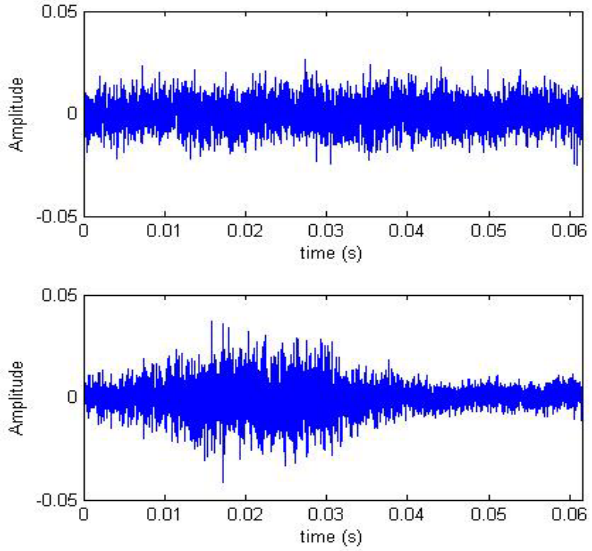

Figure 12. Healthy signal TSA (upper) and faulty signal TSA (lower)

In order to test the effectiveness and sensitiveness of different condition indicators, the following groups of condition indicators were compared:

(a) RMS, P2P, kurtosis and crest factor of the raw data.

(b) RMS, P2P, kurtosis and crest factor of the TSA data. In addition, condition indicators FM4 and NA4 were also computed using the TSA data.

(c) RMS, P2P, kurtosis and crest factor for the Teager's energy operator of the TSA.

The condition indicators calculated on the raw data without band pass filter or TSA are shown in Figure 13 through Figure 16. Note that in the experiment, 5 sets of data were collected for each input shaft speed: a total of 30 data samples were collected. They are aligned from low speed to high speed. It can be seen from Figure 13 that the raw RMS cannot separate the faulty gear from the healthy one. As the speed of the gearbox increases, the RMS increase gradually. From Figure 14, one can see that health signals have slightly larger P2P values than the faulty signals. This could be caused by the random noises, either from the misalignment of the gearbox or from the sensors. In Figure 15, it shows that the healthy signals have larger kurtosis values than the faulty signals. Based on the raw kurtosis, it is possible to separate the faulty signals from the healthy ones when the input speed is lower than 40 Hz. However at a speed higher than 40 Hz, it is impossible to distinguish healthy signals from faulty signals. Similarly in Figure 16, the healthy crest factors have larger amplitudes than faulty ones.

Based on the results of the raw data condition indicators, it is impossible to separate the health signals from the faulty ones. Also, the fact that the condition indicators of raw healthy signals have larger amplitude than the faulty condition indicators makes it impractical to set fault alarm threshold in real application.

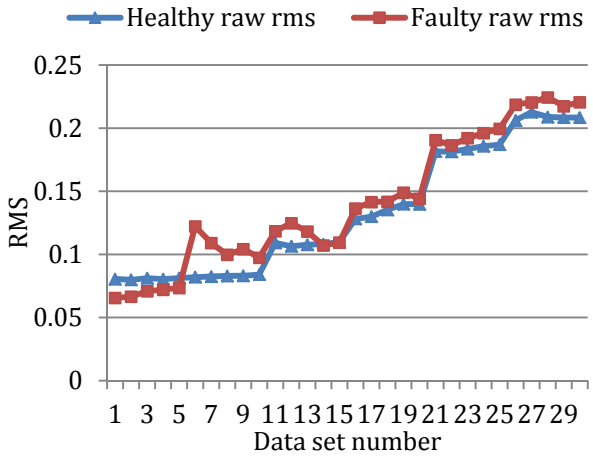

Figure 13. Raw data RMS

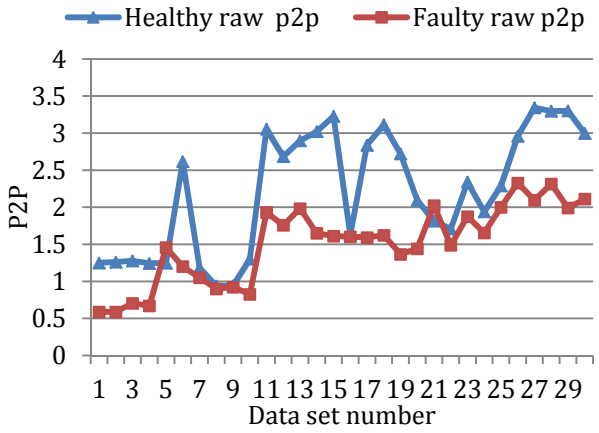

Figure 14. Raw data P2P

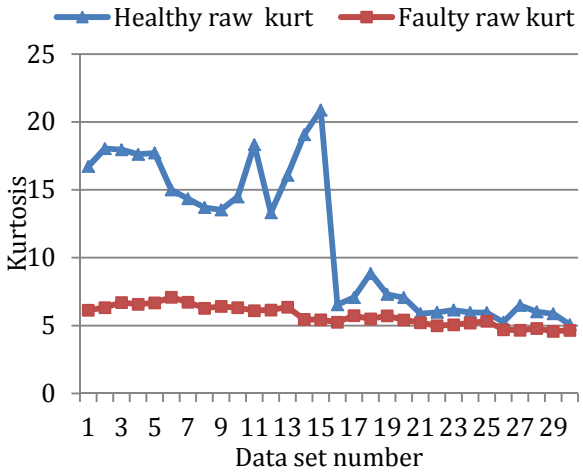

Figure 15. Raw data kurtosis

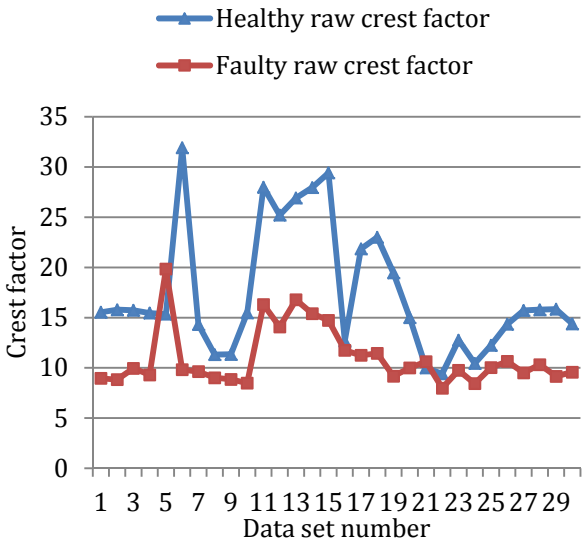

Figure 16. Raw data crest factor

In order to minimize the random noises and enhance the faulty features hidden in the raw signals, SK based filter followed by TSA was performed on the raw data.

The plots of the condition indicators computed using TSA are provided in Figure 17 through Figure 22.

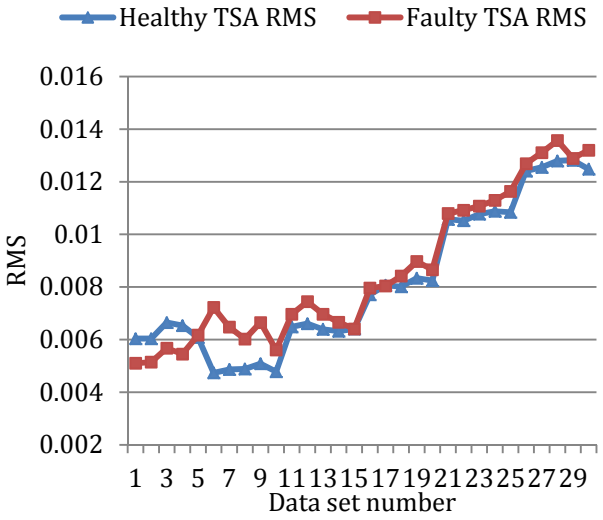

Figure 17. TSA RMS of the healthy data and faulty data

From Figure 17, one can see that the behavior of the TSA RMS is similar to that of the raw RMS in Figure 13. As the input shaft speed increases, the RMS increases for both health and faulty gears. Since both the RMS of the health signals and the RMS of the faulty signals overlap over the entire testing conditions, it is impossible to separate the gear fault using TSA RMS.

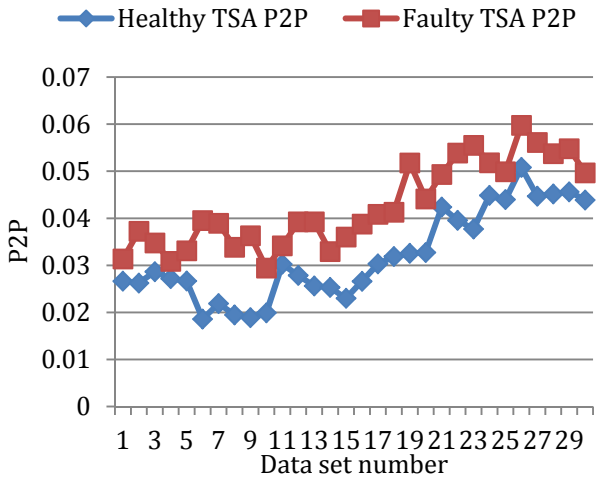

Figure 18. TSA P2P of the healthy data and faulty data

In comparison with P2P of the raw signals, one can see that the P2P of the faulty TSA signals are all larger than that of the healthy TSA signals under each individual shaft input speed, as shown in Figure 18. This confirms that the random noise is removed by TSA while the faulty features in the tooth crack condition are significantly enhanced.

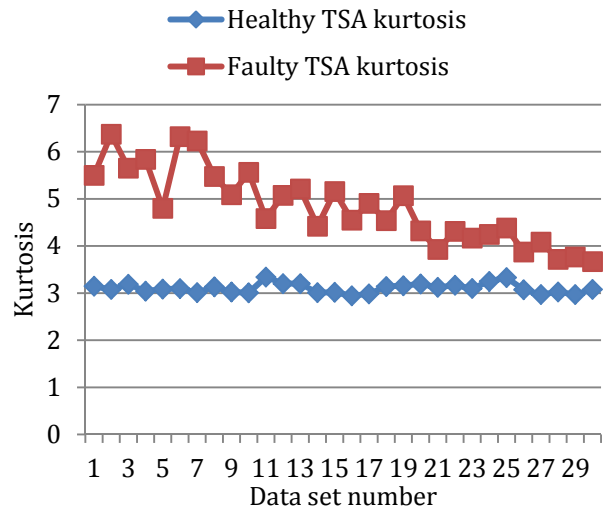

Figure 19. TSA kurtosis of the health data and tooth crack data

From Figure 19, it can be seen that the TSA kurtosis values of the health data remain almost constant around 3. As mentioned before, for any Gaussian distribution, the kurtosis is exactly calculated as 3. This concludes that the health gear TSA satisfied the Gaussian distribution. It means the amplitude of the AE impact waves generated by each tooth meshing complies with Gaussian distribution as expected. On the other hand, the TSA kurtosis of the faulty data is all above 3.6. This simply illustrates behavior of the faulty signal patterns.

Since kurtosis is non-quantitative value, it does not depend on the absolute amplitude. Kurtosis can serve as a reliable condition indicator for gearbox fault detection under variable loads and speeds.

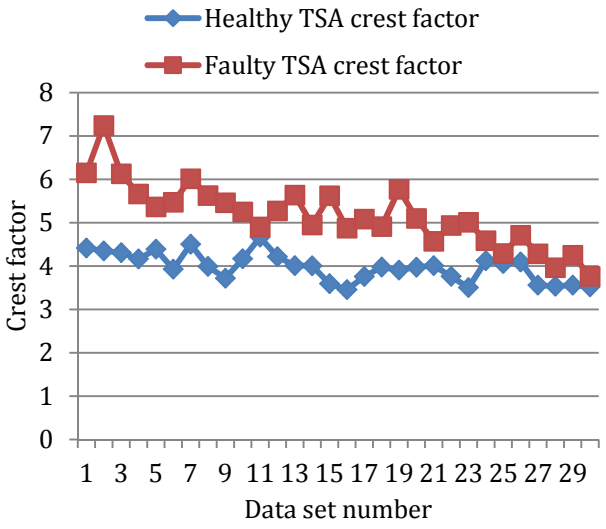

Figure 20. TSA crest factor of the healthy data and faulty data

The crest factor shows the statistics of the peak and the mean amplitude ratio. As show in Figure 20, all of the faulty TSA crest factors are larger than their health counterparts. Even though the differences of the crest factors between the healthy and faulty signals shown in Figure 20 are not as significant as those shown in Figure 19, the TSA crest factor still can be used as an effective condition indicator for detecting the gear fault.

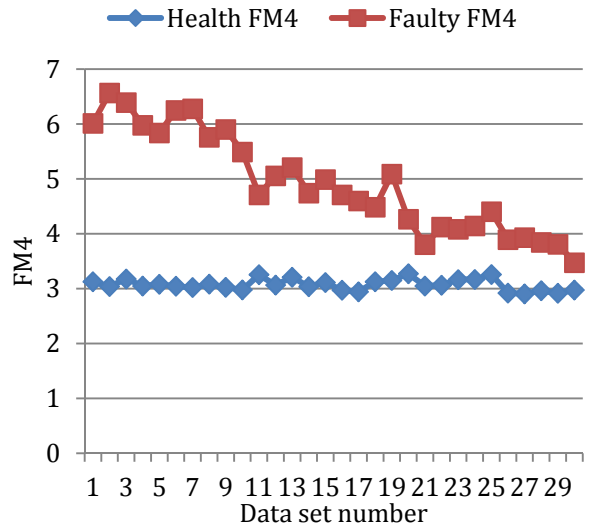

Figure 21. TSA FM4 of the health data and tooth crack data

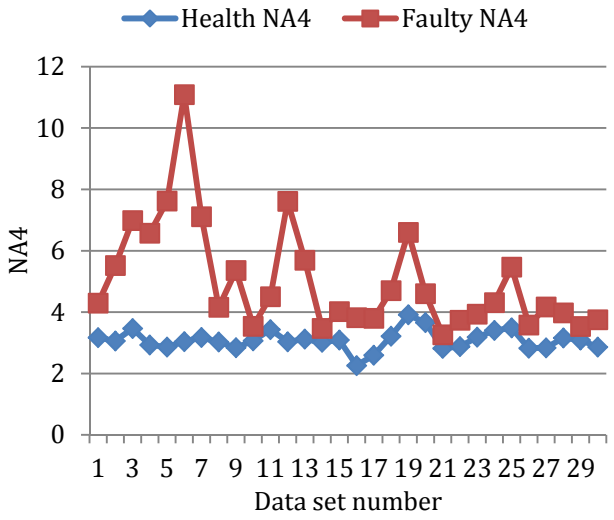

Figure 22. TSA NA4 of health and tooth crack data

Figure 21 and Figure 22 show the plots of the FM4 and NA4 condition indicators, respectively. FM4 is the difference signal kurtosis while NA4 is the residual signal kurtosis. From Figure 21, the healthy data FM4 identified itself as near Gaussian distribution. The faulty FM4 is larger which indicates fault feature. For NA4 in Figure 22, the condition indicator has more fluctuation because the variance was averaged across each 5 sets of data at each operational speed.

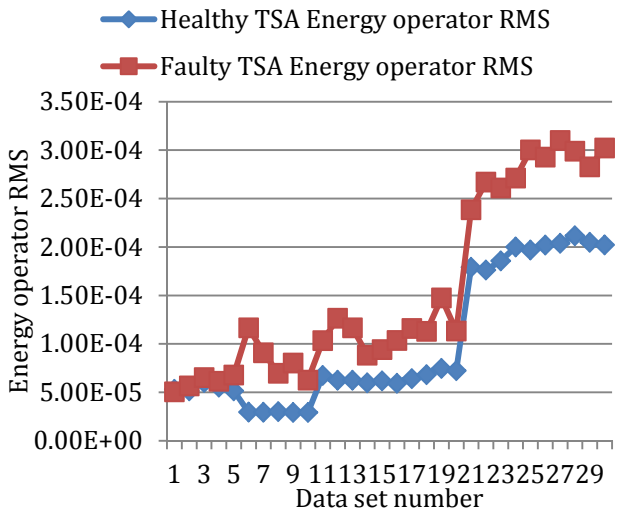

Figure 23. Energy operator RMS of healthy and tooth crack TSA data

From the above shown results of the condition indicators computed on the raw signals and TSA signals, RMS cannot separate the healthy signals from the faulty signals. Surprisingly, when taking the energy operator, one could actually see that faulty signal RMS values clearly separate

themselves from the healthy signal RMS values as the speed increases, as shown in Figure 23.

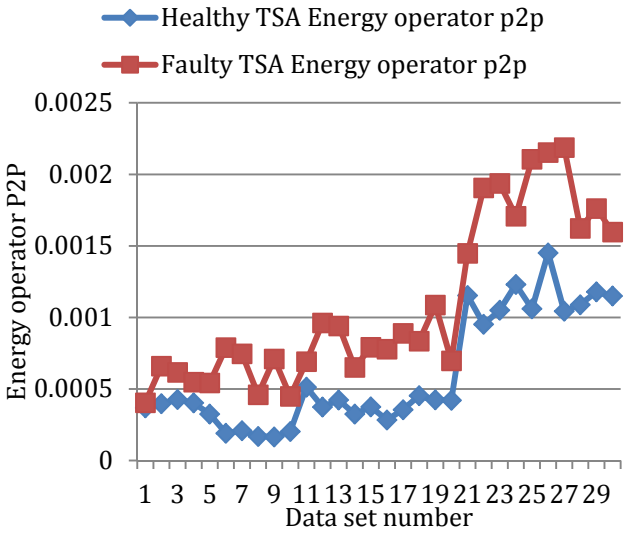

Figure 24. Energy operator P2P of healthy and tooth crack TSA data

Figure 24 shows the P2P values of the TSA energy operators. The P2P condition indicator could roughly separate the faulty signals from the healthy signals.

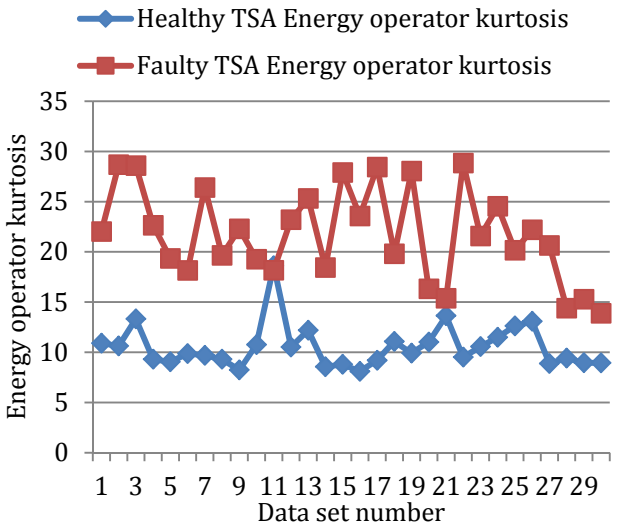

Figure 25. Energy operator kurtosis of healthy and tooth crack TSA data

Figure 25 shows the energy operator for both cases. Energy operator by definition is another kurtosis based condition indicator. From the plot, it is easy to see that energy operator can basically separate the healthy gear from the faulty gear.

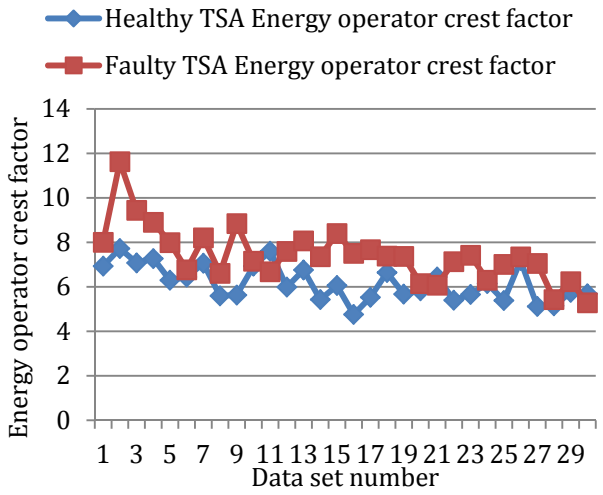

Figure 26. Energy operator crest factor of healthy and tooth crack TSA data

Figure 26 plots the TSA energy operator crest factor. It could be seen from the plot that the faulty signal crest factors are roughly larger than the healthy ones. However, there are some overlaps in a few samples. Based on the experiment results, crest factors are less reliable than kurtosis in term of tooth crack detection.

It was observed that as the gearbox speed increase, the kurtosis based condition indicators generally decrease. Two reasons might count for these behaviors. The first reason is that when the gearbox input shaft speed increases, the variance value in the denominator of Eq. (12) – Eq. (14) increases rapidly, which results in a decrease of the kurtosis based condition indicators. The second reason is that when an incipient fault is presented, the fault features are relatively small. When the gearbox is operating at a high speed, the normal gear meshing has similar impact amplitude as the fault feature, which overwhelms the fault feature. As noted, an AE signal tends to display more Gaussian type characteristics. For gear fault detection using AE signals, this might be a shortcoming at high shaft rates because AE signal amplitudes increase significantly with speed. The high amplitude of the normal gear meshing impact signals might overwhelm the incipient fault features.

Conversely, in the high shaft speed conditions, the RMS and P2P of the energy operator give clear indication for the faulty signals. The energy operator RMS and P2P of the fault signals increase much faster than the healthy signals. So it is possible to use these condition indicators to compensate the performance degradation of kurtosis based condition indicators.

One solution to this problem is to substitute the denominator with the variance of a gearbox in good condition, which then leads to the condition indicator NA4* (Lebold *et al.*, 2000). NA4* is more suitable for continuous monitoring.

In the case of naturally grown fault, it is convenient to use the variance when the gearbox is new and under good condition. The evolution of the fault growth will be easily observed. On the other hand, while this phenomenon is not exactly as desired in a high speed operational condition (1000 RPM or higher), it may benefit the detection of gearbox fault operated at lower speed (within 1000 RPM).

In summary, the condition indicators on the raw AE data did not convey much useful information for fault detection. The SK filter and TSA greatly enhanced the fault features. Most of the condition indicators on the TSA could clearly separate the faulty condition signals and healthy signals: the TSA kurtosis and FM4 worked the best in this tooth crack fault detection experiment. Furthermore, the Teager's energy operator based condition indicators could successfully separate the faulty signals from the healthy gear signals. Teager's energy operator had significant improvement on the RMS condition indicator. In addition, Teager's energy operator improved the separation between healthy TSA kurtosis and faulty TSA kurtosis.

5. CONCLUSIONS

In order to reduce wind energy costs, PHM of wind turbine is needed to reduce the operations and maintenance costs associated with running a wind farm. One of the major costs on wind turbine repairs is due to gearbox failure. Therefore, developing effective gearbox fault detection tools is important to the PHM of wind turbine.

In this paper, a new AE sensor based gear fault detection approach was presented. This new approach combines a heterodyne based frequency reduction technique with TSA and spectral kurtosis to process AE sensor signals and extract features as condition indictors for gear fault detection. Heterodyne technique commonly used in communication is first employed to preprocess the AE signals before sampling. By heterodyning, the AE signal frequency is down shifted from several hundred kHz to below 50 kHz. This reduced AE signal sampling rate is comparable to that of vibration signals.

The approach presented in this paper is physics based. The presented approach was validated using seeded gear tooth crack fault tests on a notational split torque gearbox. Condition indicators, such as RMS, P2P, kurtosis, and crest factor, were computed from the raw signals, TSA signals, and Teager's energy operator signals, separately. The results showed that the condition indicators computed on the TSA signals and Teager's energy operators could effectively separate the faulty signals from the healthy signals. Among all the condition indicators tested, kurtosis related condition indicators, like, TSA kurtosis, FM4, and Teager's energy operator kurtosis, have showed the best performance of detecting the gear tooth crack for all the testing conditions.

REFERENCES

Al-Balushi K.R., SamantaB. (2002), "Gear fault diagnosis using energy-based features of acoustic emission signals", Proceedings of the Institution of Mechanical Engineers. Part I: Journal of Systems and Control Engineering, Vol.216, No. 3, pp. 249 – 263.

Al-Ghamd, A.M. and Mba, D. (2006), "A comparative experimental study on the use of acoustic emission and vibration analysis for bearing defect identification and estimation of defect size", *Mechanical Systems and Signal Processing*, Vol. 20, No. 7, pp. 1537 – 1571.

Antoni J. (2006), "The spectral kurtosis: a useful tool for characterizing non-stationary signals", *Mechanical Systems and Signal Processing*, Vol. 20, No. 2, pp. 282–307.

Antoni J. and Randall R.B. (2006), "The spectral kurtosis: application to the vibratory surveillance and diagnostics of rotating machines", *Mechanical Systems and Signal Processing*, Vol. 20, No. 2, pp. 308–331.

Bonnardot F., Badaoui M. El, Randall R.B., Daniere J., and Guillet F. (2005), "Use of the acceleration signal of a gearbox in order to perform angular resampling (with limited speed fluctuation) ", *Mechanical Systems and Signal Processing*, Vol. 19, No. 4, pp. 766 - 785.

Braun S. (1975), "The exaction of periodic waveforms by time domain averaging", *Acustica*, Vol. 32, No.2, pp. 69 - 77.

Capdevielle V., Servie`re C., and Lacoume J.-L. (1996), Blind separation of wide-band sources: application to rotating machine signals, Proceedings of the Eighth European Signal Processing Conference, vol. 3, pp. 2085–2088.

Dwyer R.F. (1983) "Detection of non-Gaussian signals by frequency domain kurtosis estimation", *Proceedings of the International Conference on Acoustic, Speech, and Signal Processing*, Vol. 8, pp. 607–610.

Eftekharnejad B., Carrasco M.R., Charnley B., and Mba D. (2011), "The application of spectral kurtosis on Acoustic Emission and vibrations from a defective bearing", *Mechanical Systems and Signal Processing*, Vol. 25, No. 1, pp. 266 - 284.

Gao L., Zai F., Su S., Wang H., Chen P., and Liu L., (2011), "Study and Application of Acoustic Emission Testing in Fault Diagnosis of Low-Speed Heavy-Duty Gears", *Sensor*, Vol.11, No.1, pp. 599 – 611.

He D., Li R., Zhu J., and Zade M. (2011), "Data Mining Based Full Ceramic Bearing Fault Diagnostic System Using AE Sensors", *IEEE Transactions on Neural Network*, Vol. 22, No. 12, pp. 2022 – 2031.

Kaiser J. F. (1990), "On Teager's Energy Algorithm and Its Generalization to Continuous Signals", Proc. 4th IEEE Digital Signal Processing Workshop, Mohonk (New Palts), NY.

Kilundu B., Chiementin X., Duez J. and Mba D., (2011), "Cyclostationarity of Acoustic Emissions (AE) for monitoring bearing defects", *Mechanical Systems and Signal Processing*, Vol. 25, No. 6, pp.2061 - 2072.

Lebold, M.; McClintic, K.; Campbell, R.; Byington, C.; Maynard, K. (2000), Review of Vibration Analysis Methods for Gearbox Diagnostics and Prognostics, *Proceedings of the 54th Meeting of the Society for Machinery Failure Prevention Technology*, Virginia Beach, VA, May 1-4, pp. 623-634.

Li R. and He D. (2012), "Rotational Machine Health Monitoring and Fault Detection Using EMD-Based Acoustic Emission Feature Quantification", *IEEE Transactions on Instrumentation and Measurement* , Vol. 61, No.4 , pp. 990 – 1001.

Mba D. (2003), "Acoustic Emissions and monitoring bearing health", *Tribology Transactions*, Vol.46, No.3, pp. 447 – 451.

McFadden P.D. (1987), "A revised model for the extraction of periodic waveforms by time domain averaging", *Mechanical Systems and Signal Processing*, Vol.1, No.1, pp. 83 – 95.

McFadden P.D. , Toozhy M.M. (2000), "Application of synchronous averaging to vibration monitoring of rolling element bearings", *Mechanical Systems and Signal Processing*, Vol. 14, No. 6, pp.891 – 906.

Pandya D. H., , Upadhyay S.H., and Harsha S.P., (2013), "Fault diagnosis of rolling element bearing with intrinsic mode function of acoustic emission data using APF-KNN", *Expert Systems with Applications*, http://dx.doi.org/10.1016/j.eswa.2013.01.033

Teager H. M. and Teager S. M. (1992), "Evidence for Nonlinear Sound Production Mechanisms in the Vocal Tract", in Speech Production and Speech Symp. Time-Frequency and Time-Scale Analysis, Victoria, British Columbia, Canada, pp. 345-348.

Večeř P., Kreidl M. and Šmíd R. (2005), "Condition Indicators for Gearbox Condition Monitoring Systems", *Acta Polytechnica*, Vol. 45, No. 6, pp. 35 - 43.

Zakrajsek J.J., Townsend D.P., Decker H.J. (1993), "An analysis of gear fault detection methods as applied to pitting fatigue failure data", Technical Report NASA TM-105950, AVSCOM TR-92-C-035, *NASA and the US Army Aviation Systems Command*.

BIOGRAPHIES

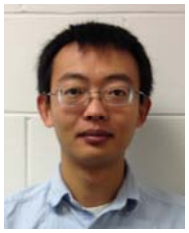

Yongzhi Qu received his B.S. in Measurement and Control and M.S. in Measurement and Testing from Wuhan University of Technology, China. He is a PhD candidate in the Department of Mechanical and Industrial Engineering at The University of Illinois Chicago. His research interests include: rotational machinery health monitoring and fault diagnosis, especially with acoustic emission sensors, embedded system design and resources allocation and scheduling optimization.

Eric Bechhoefer received his B.S. in Biology from the University of Michigan, his M.S. in Operations Research from the Naval Postgraduate School, and a Ph.D. in General Engineering from Kennedy Western University. His is a former Naval Aviator who has worked extensively on condition based maintenance, rotor track and balance, vibration analysis of rotating machinery and fault detection in electronic systems. Dr. Bechhoefer is a board member of the Prognostics Health Management Society, and a member of the IEEE Reliability Society.

David He received his B.S. degree in metallurgical engineering from Shanghai University of Technology, China, MBA degree from The University of Northern Iowa, and Ph.D. degree in industrial engineering from The University of Iowa in 1994. Dr. He is a Professor and Director of the Intelligent Systems Modeling & Development Laboratory in the Department of Mechanical and Industrial Engineering at The University of Illinois-Chicago. Dr. He's research areas include: machinery health monitoring, diagnosis and prognosis, complex systems failure analysis, quality and reliability engineering, and manufacturing systems design, modeling, scheduling and planning.

Junda Zhu received his B.S. degree in Mechanical Engineering from Northeastern University, Shenyang, China, and M.S. degree in Mechanical Engineering from The University of Illinois at Chicago in 2009. He is a Ph.D. candidate at the Department of Mechanical and Industrial Engineering. His current research interests include lubrication oil condition monitoring and degradation simulation and analysis, rotational machinery health monitoring, diagnosis and prognosis with vibration or acoustic emission based signal processing techniques, physics/data driven based machine failure modeling, CAD and FEA.